Faculty and Researchers | Faculty and Researchers' Publications

2018

Relationships Between Maneuver Time and Energy for Reaction Wheel Attitude Control

Marsh, Harleigh C.; Karpenko, Mark; Gong, Qi

AIAA

Relationships Between Maneuver Time and Energy for Reaction Wheel Attitude Control

Harleigh C. Marsh*
University of California, Santa Cruz, Santa Cruz, California 95064
Mark Karpenko†
Naval Postgraduate School, Monterey, California 93943
and
Qi Gong‡
University of California, Santa Cruz, Santa Cruz, California 95064

The dichotomy between minimum time and minimum effort is well known. Minimum-time solutions are synonymous with large effort, whereas minimum effort solutions imply large time horizons. Shortest-time attitude maneuvers are minimum-time slews for agile reorientation of space vehicles. Intuition and experience would suggest that such maneuvers are expensive in terms of effort. This paper will show that this is not the case: Agile maneuvers exist within the energy budget associated with conventional attitude control systems. Moreover, even for conventional slew strategies (such as eigenaxis), energy requirements can be reduced. The energy savings are realized via a reallocation of the control effort by exploiting null motions within the control space, over the maneuver trajectory. A cost functional for minimum-energy slews is developed that is in line with true energy cost associated with reaction wheel-based attitude control systems. This energy metric is incorporated into a family of constrained nonlinear optimal control formulations whose solutions present a relationship between transfer time and energy. Both agile (off-eigenaxis) slews and conventional (eigenaxis) slews are studied. A trade space between transfer time and energy is identified, which can be exploited for mission operations, planning, and design.

I. Introduction

MINIMUM-TIME attitude maneuvers have been widely studied in the literature. The survey paper by Scrivener and Thompson [1] describes the state of the art up to 1994. The early work, which focused largely on kinematic motion planning (under the assumption of a spherical inertia tensor), showed that the slew time improvement was typically small (less than 1% for a 30 deg maneuver) [2]. Later, Shen and Tsiotras [3] and Proulx and Ross [4] studied minimum-time maneuvering for the cases of axisymmetric and nonsymmetric rigid bodies, respectively. In this work, higher performance was obtained by considering the full dynamics of the spacecraft. Fleming [5] and Fleming et al. in [6–9] further advanced the analysis to the more realistic cases of spacecraft equipped with various actuators, from magnetic torquers to reaction wheels and control moment gyros. In 2010, flight tests on the TRACE spacecraft showed that shortest-time maneuvers (slews designed to exploit the spacecraft dynamics) can indeed enhance the performance of practical space systems [10,11].

In the aforementioned body of work, the primary focus was on enhancing spacecraft agility by reducing maneuver time. Experience and intuition would suggest that the price to be paid for a reduction in slew time is a significant increase in the energy that must be expended to execute the slew. Energy is a fundamentally limited resource of a spacecraft, directly affecting its utility and mission life. With this in mind, operational implementation of intuitively "inefficient" agile

maneuvers may seem contrary to the stringent requirements on the size, weight, and power of a satellite attitude control system. The goal of this paper is to explore the relationship between maneuver time and energy for reaction wheel attitude control to determine the boundaries of the energy budget for agile attitude control. To accomplish this task, it is necessary to identify suitable energy metrics for measuring the consumption of agile maneuvering schemes. Existing research on minimum-energy attitude maneuvers for reaction wheel spacecraft has been approached from a variety of perspectives concerning the way in which reaction wheel power is modeled and whether energy consumption is minimized instantaneously (a local approach) or over an entire trajectory (a global approach).

The local approach minimizes the instantaneous reaction wheel power by static optimization. In the literature, various proxies for instantaneous reaction wheel power have been employed. In [12,13], solutions were developed that minimize the reaction wheel mechanical power for a spacecraft with a redundant actuator array. This was done by allocating the body frame control torques determined by a given attitude control law to the individual reaction wheels. In [12], the L^2 norm of reaction wheel mechanical power $\tau\Omega$ was minimized, whereas in [13], mechanical power was minimized under the assumption that mechanical energy may be extracted when braking a wheel. The instantaneous L^1 norm of mechanical power was considered in [14] as a part of a dissipative power reduction allocation scheme.

The global approach minimizes the energy over the entire maneuver trajectory (i.e., the integral of the instantaneous power) by constructing and solving an optimal control problem [15–17]. For example, in [15], the cost functional was constructed to minimize the integrated reaction wheel copper loss $I^2 R$, the current-squared times winding resistance. Reaction wheel friction losses were not considered, and so minimizing the copper loss was analogous to minimizing the L^2 norm of the reaction wheel motor torque τ. Global optimization using a quadratic performance index based on reaction wheel mechanical power was considered in [16] for a single-wheel slew and in [17] for a three-wheel array. In reality, a model for reaction wheel power consumption is more complicated than the simplified models based on mechanical power or copper loss would suggest. Three terms should be considered simultaneously: the copper loss, friction loss, and mechanical power. A complication,

---

*Ph.D. Candidate, Department of Applied Mathematics & Statistics; hcmarsh@soe.ucsc.edu. Student Member AIAA.
†Research Associate Professor, Department of Mechanical and Aerospace Engineering; mkarpenk@nps.edu. Member AIAA.
‡Associate Professor, Department of Applied Mathematics and Statistics; qigong@soe.ucsc.edu.

however, is that such a model additionally requires that only the positive part of the reaction wheel power be considered because energy is only consumed when the wheel motors act as a load. Energy generated when the wheel motors act as sources, the negative part of the power equation, is typically shunted to ground. The resulting nonsmooth optimal control problem can be challenging to solve, thus motivating the use of proxies for power as described earlier.

In this paper, the relationship between maneuver time and energy for a practical reaction wheel attitude control system is studied. The total amount of energy consumed to complete a slew is computed by identifying, at each instant of time, whether a motor is acting as a consumer or a generator and integrating only the positive part of the reaction wheel power equations. It is observed that, for a zero-net bias momentum control system, where the reaction wheels are operated about a nominally fixed bias rate, the reaction wheel electrical power input equation can be reduced to a quadratic form comprising only dissipative terms. Thus, a smooth cost functional can be written based on the cumulative dissipative losses. This energy metric is incorporated into a constrained nonlinear optimal control formulation that is solved using pseudospectral optimal control theory [18]. The constructed optimal control problem formulation directly considers the nonlinear dynamics of the rotating spacecraft, along with state and control constraints pertinent to an operational environment, for example, reaction wheel speed bias, limits on achievable torque and momentum, as well as saturation of the rate gyros. The relationship between transfer time and energy is determined by solving a series of fixed-time problems for both agile (off-eigenaxis) slews and conventional (eigenaxis) slews. The results indicate that agile maneuvers can, in fact, be performed within the energy budget associated with a conventional attitude control system, a counterintuitive result. Moreover, energy requirements for conventional slew strategies (such as eigenaxis) can be reduced. The dichotomy between minimum time and minimum effort is addressed via the additional degrees of freedom associated with the redundant reaction wheel array. In particular, the results show that the energy savings are realized via a reallocation of the control effort by exploiting null motions within the control space. Thus, a trade space between transfer time and energy exists that can be exploited for mission operations, planning, and design.

The remainder of this paper is organized as follows. In Sec. II, a set of optimal control problems are formulated to minimize the energy required to perform a rest-to-rest maneuver under various constraints in line with an operational setting. Section III analyzes the minimum-energy maneuvers, and elaborates on the mechanism for energy reduction by an analysis of the reaction wheel null space. Section IV presents the results on the nonlinear relationship between transfer time and energy required to perform a maneuver for both agile (off-eigenaxis) and conventional (eigenaxis) slews. The trade space between energy and transfer time between for various maneuver types is identified and explored. Finally, conclusions are given in Sec. V.

II. Minimum-Energy Problem Formulation

This section presents the development of an optimal control problem formulation to minimize the energy required to perform reaction wheel attitude maneuvers under various constraints. First, the rotational dynamics of the spacecraft is briefly reviewed. Operation of the reaction wheel motors is described next so that appropriate metrics for electrical energy consumption can be derived. Finally, the optimal control problem is formulated and the necessary conditions associated with Pontryagin's minimum principle are derived.

A. Spacecraft Attitude Control Model

Consider a spacecraft with N_{rw} reaction wheels. The total angular momentum $H \in \mathbb{R}^3$ of the spacecraft system with respect to the body-fixed frame can be decomposed as

$$H = H_{sc} + H_{rw} \qquad (1)$$

where $H_{sc} \in \mathbb{R}^3$ is the total angular momentum of the spacecraft, and $H_{rw} \in \mathbb{R}^3$ is the total angular momentum of the reaction wheels projected into the body-fixed frame. Vectors H_{sc} and H_{rw} are

$$H_{sc} = J_{sc}\omega \qquad (2)$$

$$H_{rw} = Ah_{rw} \qquad (3)$$

where $J_{sc} \in \mathbb{R}^{3 \times 3}$ is the spacecraft inertia tensor, $\omega \in \mathbb{R}^3$ is the angular velocity of the spacecraft, $A = [a_1| \cdots |a_{N_{rw}}] \in \mathbb{R}^{3 \times N_{rw}}$ is the reaction wheel projection matrix, and $h_{rw} \in \mathbb{R}^{N_{rw}}$ is the reaction wheel angular momentum vector referenced to the individual wheel spin axes.

Defining $J_{rw} \in \mathbb{R}^{N_{rw} \times N_{rw}}$ as a diagonal matrix, whose ith entry is the inertia of the ith reaction wheel, and defining the angular rates of the reaction wheels relative to their spin axes as $\Omega_{rw} \in \mathbb{R}^{N_{rw}}$ gives

$$h_{rw} = J_{rw}(\Omega_{rw} + A^T\omega) \qquad (4)$$

where the term $J_{rw}A^T\omega$ accounts for the angular momentum increment resulting from the motion of the spacecraft relative to the wheels. Because reaction wheels are normally operated at a bias rate, $\Omega_{rw,i} \gg a_i^T\omega$, and so Eq. (4) may be approximated as

$$h_{rw} = J_{rw}\Omega_{rw} \qquad (5)$$

The time rate of change with momentum in the body-fixed frame is determined by the application of the transport theorem [19]. Assuming that J_{sc}, J_{rw}, and A are time invariant, we have

$$\dot{H}_{sc} = J_{sc}\dot{\omega} + \omega \times J_{sc}\omega \qquad (6)$$

$$\dot{H}_{rw} = A\tau_{rw} + \omega \times AJ_{rw}\Omega_{rw} \qquad (7)$$

where $\tau_{rw} = J_{rw}\dot{\Omega}_{rw} \in \mathbb{R}^{N_{rw}}$ is the torque generated by each reaction wheel about its spin axis. Assuming the absence of external disturbance torques, angular momentum is conserved and the time rate of change to the system's total angular momentum with respect to the inertial frame is null. Thus, $\dot{H}_{sc} + \dot{H}_{rw} = 0$, giving

$$J_{sc}\dot{\omega} = -A\tau_{rw} - \omega \times (J_{sc}\omega + AJ_{rw}\Omega_{rw}) \qquad (8)$$

Combining Eq. (8) with the derivative of Eq. (5), the rotational dynamics of the spacecraft with N_{rw} wheels can be written in the following matrix form:

$$\begin{bmatrix} \dot{\omega} \\ \dot{\Omega}_{rw} \end{bmatrix} = \begin{bmatrix} J_{sc}^{-1}(-A\tau_{rw} - \omega \times (J_{sc}\omega + AJ_{rw}\Omega_{rw})) \\ J_{rw}^{-1}\tau_{rw} \end{bmatrix}$$

To complete the spacecraft model, the attitude of the spacecraft is represented using quaternions parameterized as

$$q = \left[e_1 \sin\left(\frac{\Phi}{2}\right), \quad e_2 \sin\left(\frac{\Phi}{2}\right), \quad e_3 \sin\left(\frac{\Phi}{2}\right), \quad \cos\left(\frac{\Phi}{2}\right) \right]^T \in \mathbb{R}^4$$

where $e = [e_1, e_2, e_3]^T$ is the eigenaxis and Φ is the rotation angle about the eigenaxis. The quaternion kinematic differential equations are described by the following system [20]:

$$\dot{q} = \frac{1}{2}\mathcal{Q}(\omega)q$$

where $\mathcal{Q}(\omega)$ is a skew-symmetric matrix given as

$$\mathcal{Q}(\omega) \triangleq \begin{bmatrix} 0 & \omega_3 & -\omega_2 & \omega_1 \\ -\omega_3 & 0 & \omega_1 & \omega_2 \\ \omega_2 & -\omega_1 & 0 & \omega_3 \\ -\omega_1 & -\omega_2 & -\omega_3 & 0 \end{bmatrix}$$

B. Electrical Energy Model and Energy Metrics

From the point of view of minimizing energy consumption for slew, it is reasonable to model the electric motor of a reaction wheel as a dc motor in steady state. Thus, it is assumed that inductive losses are small compared with the dc power loss in the windings. In the steady state, the load torque is taken as the sum of the commanded-torque τ_{rw} and a speed-dependent friction term. The angular velocity of the motor shaft is taken as the speed of the reaction wheel Ω. Under these assumptions, the steady-state dc motor equations are

$$V = IR + K_V\Omega, \quad K_T I = \tau_{\text{rw}} + \beta\Omega$$

In the preceding equations, V is armature voltage, I is the armature current, R is the armature resistance, K_V is the back electromotive force (EMF) constant, K_T is the motor torque constant, and β is the viscous friction coefficient. For SI units, we note that $K_T = K_V$. When determining the electrical power at any instant in time, three terms appear: an armature copper-loss term that represents power lost as heat in the windings, a mechanical power term, and a term representing the dissipative loss due to friction:

$$\mathcal{P}(t) = V(t)I(t) = I^2(t)R + K_V\Omega(t)I(t),$$
$$= \underbrace{\frac{R}{K_T^2}(\tau_{\text{rw}}(t) + \beta\Omega(t))^2}_{\text{Copper Loss}} + \underbrace{\tau_{\text{rw}}(t)\Omega(t)}_{\text{Mechanical Power}} + \underbrace{\beta\Omega^2(t)}_{\text{Friction Loss}} \quad (9)$$

During a slew, each reaction wheel motor may alternate between being a load $[\mathcal{P}_i(t) > 0]$ or acting as a source $[\mathcal{P}_i(t) < 0]$. In a regenerative system, it is assumed that the spacecraft batteries can be recharged when any motor acts as a source [12,13]. In practice, regenerative methods are not implemented, and so when a motor acts as a source, the energy is dissipated through a ballast resistor [21] and cannot be recovered. From the preceding, the total instantaneous electric power exerted for N_{rw} reaction wheels, is given as

$$\mathcal{P}^+(t) = \sum_{i=1}^{N_{\text{rw}}} \{V_i(t)I_i(t)\}^+ \quad (10)$$

where $\{\cdot\}^+$ is defined as

$$\{f(t)\}^+ = \begin{cases} f(t) & \text{if} \quad f(t) > 0 \\ 0 & \text{if} \quad f(t) \leq 0 \end{cases}$$

Integrating Eq. (10) over the transfer time $[0, T]$ thus represents the total electrical energy required to perform a slew:

$$\mathcal{E}^+ = \int_0^T \mathcal{P}^+(t)\, dt$$

Although $\mathcal{E}^+$ represents the energy consumed to perform a maneuver, taking $\mathcal{E}^+$ as the cost functional in an optimal control problem poses a numerical challenge since $\mathcal{P}^+$ is a nonsmooth function. Alternatively, for each reaction wheel, we may write $\mathcal{P}^+ = (1/2)(\mathcal{P} + |\mathcal{P}|) \leq 1/2(\tau_{\text{rw}}\Omega + |\tau_{\text{rw}}\Omega| + 2\mathcal{D}_{\text{loss}})$ where $\mathcal{D}_{\text{loss}}$ is the instantaneous dissipative loss in Eq. (9). Integrating this equation term by term (to evaluate energy consumption over a slew) gives

$$\mathcal{E}^+(T) \leq \frac{J_{\text{rw}}}{4}(\Omega_{\text{rw}}^2(T) - \Omega_{\text{rw}}^2(0)) + \int_0^T \left(\frac{|\tau_{\text{rw}}(t)\Omega_{\text{rw}}(t)|}{2}\right) dt$$
$$+ \int_0^T \left(\frac{R}{K_T^2}(\tau_{\text{rw}}(t) + \beta\Omega_{\text{rw}}(t))^2 + \beta\Omega_{\text{rw}}^2(t)\right) dt \quad (11)$$

If it is assumed that each slew begins and ends with the same wheel bias, the first term in Eq. (11) is null, leaving

$$\mathcal{E}^+(T) \leq \int_0^T \left(\frac{|\tau_{\text{rw}}(t)\Omega_{\text{rw}}(t)|}{2}\right) dt$$
$$+ \int_0^T \left(\frac{R}{K_T^2}(\tau_{\text{rw}}(t) + \beta\Omega_{\text{rw}}(t))^2 + \beta\Omega_{\text{rw}}^2(t)\right) dt \quad (12)$$

which may be further decomposed as

$$\mathcal{E}^+(T) \leq \int_0^T \left(\frac{|\tau_{\text{rw}}(t)\Omega_{\text{rw}}(t)|}{2}\right) dt + \mathcal{C}_{\text{loss}} + \mathcal{F}_{\text{loss}} \quad (13)$$

where

$$\mathcal{C}_{\text{loss}} = \int_0^T I^2(t)R\, dt \quad (14)$$

$$\mathcal{F}_{\text{loss}} = \int_0^T \Omega_{\text{rw}}^2(t)\beta\, dt \quad (15)$$

are the cumulative dissipative losses due to heating of the motor windings $\mathcal{C}_{\text{loss}}$ and wheel friction drag $\mathcal{F}_{\text{loss}}$.

From Eq. (13), it is evident that a cost functional that minimizes the dissipative losses would also tend to reduce the integral involving the absolute value because the quadratic terms penalize large values of τ_{rw} and Ω_{rw}. Therefore, minimizing the cumulative dissipative losses serves as a useful proxy for energy consumption over a slew. Thus, an appropriate smooth cost functional for optimal control is to minimize

$$\mathcal{E}_{\text{loss}}^{\text{loss}} = \sum_{i=1}^{N_{\text{rw}}} \mathcal{C}_{\text{loss},i} + \sum_{i=1}^{N_{\text{rw}}} \mathcal{F}_{\text{loss},i} \quad (16)$$

We note three remarks by taking $\mathcal{E}_{\text{total}}^{\text{loss}}$ as the cost functional: 1) Trajectories that minimize $\mathcal{E}_{\text{total}}^{\text{loss}}$ minimize dissipative losses, and therefore the amount of heat the spacecraft has to reject is minimized. 2) Although Eq. (16) ultimately provides an estimate for energy consumption, it is always possible determine the true energy consumption $\mathcal{E}^+$ for an optimized slew a posteriori for comparison with conventional maneuvers. 3) The metric $\mathcal{E}_{\text{total}}^{\text{loss}}$ serves to measure the electrical power under the assumption of a 100% regenerative scheme [22].

C. Optimal Control Problem Formulation

In this section, the energy cost functional developed in the previous section is used toward formulating an optimal control problem for minimizing the electrical energy required for slew. Rest-to-rest maneuvers (i.e., $\omega^0 = \omega^f = 0 \in \mathbb{R}^3$) from an initial orientation

$$q^0 \triangleq \left[e_0 \sin\left(\frac{\Phi_0}{2}\right), \cos\left(\frac{\Phi_0}{2}\right)\right]^T \in \mathbb{R}^4$$

to a final orientation given by

$$q^f \triangleq \left[e_f \sin\left(\frac{\Phi_f}{2}\right), \cos\left(\frac{\Phi_f}{2}\right)\right]^T \in \mathbb{R}^4$$

are considered. By a simple change of the boundary conditions, other operational slew scenarios could also be evaluated.

The optimal control problem formulation incorporates practical constraints on both the state and the control variables that are in line with typical operations: 1) The reaction wheels start and end at the same bias speeds Ω_{bias}. 2) Per axis limits, ω_{max} are imposed upon the spacecraft angular rate to avoid saturation of the rate gyros. 3) Hardware constraints are considered for the reaction wheels with respect to momentum storage Ω_{max} and maximum torque τ_{max} authority for each reaction wheel.

The optimal control problem formulation, presented as follows, is hereafter referred to as the minimum-energy (ME) formulation:

$$(\text{ME})\begin{cases} \text{State:} \quad x = [q, \omega, \Omega_{\text{rw}}]^T \in \mathbb{R}^{7+N_{\text{rw}}}, \text{Control:} u = \tau_{\text{rw}} \in \mathbb{R}^{N_{\text{rw}}}, \\[2mm] \text{Minimize:} \quad J[x(\cdot), u(\cdot)] = \int_0^T \sum_{i=1}^{N_{\text{rw}}} \left(\frac{R}{K_T^2}(\tau_{rw,i}(t) + \beta\Omega_{rw,i}(t))^2 + \beta\Omega_{rw,i}^2(t) \right) dt \\[2mm] \text{Subject to:} \\[2mm] \begin{bmatrix} \dot{q} \\ \dot{\omega} \\ \dot{\Omega}_{\text{rw}} \end{bmatrix} = \begin{bmatrix} \frac{1}{2}\mathcal{Q}(\omega)q \\ J_{\text{sc}}^{-1}\left(-A\tau_{\text{rw}} - \omega \times (J_{\text{sc}}\omega + AJ_{\text{rw}}\Omega_{\text{rw}})\right) \\ J_{\text{rw}}^{-1}\tau_{\text{rw}} \end{bmatrix} \\[2mm] x(0) = [q^0, \omega^0, \Omega_{\text{bias}}]^T \in \mathbb{R}^{7+N_{\text{rw}}}, x(t_f) = [q^f, \omega^f, \Omega_{\text{bias}}]^T \in \mathbb{R}^{7+N_{\text{rw}}} \\[2mm] |\omega_i| \le \omega_{\max}, \quad \forall\, i = 1, 2, 3 \\[2mm] |\Omega_{rw,i}| \le \Omega_{\max}, \quad \forall\, i = 1, \ldots, N_{\text{rw}} \\[2mm] |\tau_{rw,i}| \le \tau_{\max}, \quad \forall\, i = 1, \ldots, N_{\text{rw}} \end{cases} \tag{17}$$

The state space of the system consists of the attitude of the spacecraft, angular velocity of the spacecraft body, and angular velocities of the reaction wheels (about their individual spin axis). The control vector is taken as the vector of individual reaction wheel torques. The upper bound on the transfer time is given by T. For problem ME to be feasible, the value of T must be, at minimum, the transfer time of the shortest-time maneuver (denoted t_{STM}) for the same boundary conditions. For a minimum-energy problem, it is typical for the maneuver time horizon to be longer than shortest time (i.e., $T > t_{\text{STM}}$). From this point of view, a minimum-energy shortest-time maneuver can be determined by setting $T = t_{\text{STM}}$. We note that t_{STM} can be determined by a simple modification to the cost functional by rewriting $J[x(\cdot), \tau_{\text{rw}}(\cdot), t_f] = t_f$ and allowing $0 \le t \le \infty$.

Because problem ME does not impose a motion constraint to force an eigenaxis slew, off-eigenaxis motions are allowed if they are advantageous with respect to meeting a given constraint on the slew time. The analysis to follow is, however, also concerned with evaluating the energy requirements of eigenaxis slew profiles against the conventional eigenaxis control logic [20]. To achieve an eigenaxis maneuver under a slew rate constraint, the ME formulation presented in Eq. (17) requires two modifications. To constrain the motion of the

pseudospectral optimal control theory [18,24–26] implemented in DIDO [27]. An attractive feature of pseudospectral optimal control theory is the ability to generate adjoint variables from the numerical solutions via the Covector Mapping Theorem [28–30]. This enables the verification of the optimality of numerical solutions against Pontryagin's minimum principle. In the next section, we briefly describe some key necessary optimality conditions. Propagation tests (see [27]) should also be performed to verify the convergence of each solution.

D. Necessary Conditions for Optimality

For the sake of brevity, only the necessary conditions pertaining to problem ME, given in Eq. (17), are considered in this section. The necessary conditions for the variants of problem ME may be derived analogously.

At the heart of the Pontryagin's minimum principle is the Hamiltonian minimization condition (HMC). The HMC requires for an extremal control $u^* = \tau_{\text{rw}}$ to be optimal, that u^* must minimize the control Hamiltonian at each instant of time. Let $\lambda_q \in \mathbb{R}^4$, $\lambda_\omega \in \mathbb{R}^3$, $\lambda_\Omega \in \mathbb{R}^{N_{\text{rw}}}$ be the costate variables for the respective states. The HMC for problem ME can be summarized as

$$(\text{HMC})\begin{cases} \text{Min:} \quad H(\lambda, x, u) = P_{\text{total}}^{\text{loss}}(x, u) + \left[\lambda_q^T, \lambda_\omega^T, \lambda_\Omega^T\right]\begin{bmatrix} \frac{1}{2}\mathcal{Q}(\omega)q \\ J_{\text{sc}}^{-1}(-Au - \omega \times (J_{\text{sc}}\omega + AJ_{\text{rw}}\Omega_{\text{rw}})) \\ J_{\text{rw}}^{-1}u \end{bmatrix} \\[2mm] \text{Subject to:} \quad -\omega_{\max} \le \omega_i \le \omega_{\max}, \quad \forall\, i = 1, 2, 3 \\[2mm] \qquad\qquad -\Omega_{\max} \le \Omega_i \le \Omega_{\max}, \quad \forall\, i = 1, \ldots, N_{\text{rw}} \\[2mm] \qquad\qquad -\tau_{\max} \le u_i \le \tau_{\max}, \quad \forall\, i = 1, \ldots, N_{\text{rw}} \end{cases}$$

spacecraft, the angular velocity vector of the spacecraft must always be collinear with the eigenaxis [23]. Including the following path constraint as part of problem ME achieves this goal:

$$\omega(t) \times e = 0 \in \mathbb{R}^3, \quad \forall t$$

It is also necessary to enforce a spherical slew rate constraint. This can be done by including an additional path constraint of the form $\|w\| \le \omega_{\max}$. By inserting these two path constraints, both a shortest-time eigenaxis-constrained maneuver, as well as a minimum-energy eigenaxis maneuver (ME-EAM) may be determined.

Problem ME and its variants may be readily solved using computational optimal control algorithms. In this paper, we use the

where

$$\mathcal{P}_{\text{total}}^{\text{loss}}(x, u) = \sum_{i=1}^{N_{\text{rw}}} \frac{R}{K_T^2}(\tau_{rw,i} + \beta\Omega_{rw,i})^2 + \beta\Omega_{rw,i}^2$$

An application of the Karush–Kuhn–Tucker (KKT) conditions on the HMC results in the following complementarity conditions, which require each component of ω, Ω, u and the associated KKT multipliers $\mu \triangleq [\mu_\omega, \mu_\Omega, \mu_u]^T \in \mathbb{R}^{3+2N_{\text{rw}}}$ to satisfy

$$\mu_{\omega_i} \begin{cases} \leq 0 & \omega_i = -\omega_{\max} \\ = 0 & -\omega_{\max} < \omega_i < \omega_{\max} \\ \geq 0 & \omega_i = \omega_{\max} \end{cases}, \quad \mu_{\Omega_i} \begin{cases} \leq 0 & \Omega_{rw,i} = -\Omega_{\max} \\ = 0 & -\Omega_{\max} < \Omega_{rw,i} < \Omega_{\max} \\ \geq 0 & \Omega_{rw,i} = \Omega_{\max} \end{cases},$$

$$\mu_{u_i} \begin{cases} \leq 0 & u_i = -\tau_{\max} \\ = 0 & -\tau_{\max} < u_i < \tau_{\max} \\ \geq 0 & u_i = \tau_{\max} \end{cases} \tag{18}$$

Furthermore, the Hamiltonian evolution condition requires that the lower Hamiltonian be constant for all time [i.e., $(\partial \mathcal{H}/\partial t) = 0 \; \forall t$].

To illustrate the application of the complementarity condition and Hamiltonian evolution condition as tests for optimality, problem ME was solved for a 180 deg z-axis slew. The associated spacecraft parameters are given in the Appendix. The maneuver time was taken to be $T = 279.9$ s (the minimum transfer time for this particular maneuver), thereby considering a minimum-energy shortest-time maneuver. The solution gave a value for $\mathcal{E}^+$ as 143.9 J. The associated attitude, angular rate, and reaction wheel speed profiles are shown in Fig. 1. The analysis of the minimum-energy shortest-time maneuvers is compared with standard shortest-time maneuvers in Sec. III.A.

Figure 2 shows the satisfaction of the necessary conditions for the maneuver of Fig. 1. The time history of the lower Hamiltonian is shown in Fig. 2a. For a minimum-time problem, Pontryagin's minimum principle states that the value of the lower Hamiltonian should be -1 over the entire time horizon $[0, T]$. Although the lower Hamiltonian in Fig. 2a is observed to be nominally constant, as required by the Hamiltonian evolution condition, the value is not -1 as predicted by the minimum principle. This discrepancy is a result of the fact that problem ME was solved as a fixed-time problem instead of a minimum-time problem. For the case of a fixed-time problem, the transversality conditions admit other constant values for the Hamiltonian. Hence, the value $\mathcal{H}(t) = -36.1$ J/s in Fig. 2a satisfied the necessary condition. Figure 2b shows the complementarity condition on the spacecraft angular rate ω_2. As can be seen, the KKT multiplier varies in accordance with Eq. (18), which specifies that $\mu_{\omega_i} = 0$ unless the constraint on ω_i is active. Profiles for the other spacecraft body axes are similar, and so the results are omitted for brevity. The specifics on the other necessary conditions, such as the details on transversality, Hamiltonian value conditions, etc., although verified, have been omitted for brevity.

In addition to verifying the satisfaction of the necessary conditions for each candidate optimal control solution, it is also necessary to demonstrate the feasibility of candidate optimal control u^* to fully vet the numerical solutions (see the discussion on verification and validation in Ross [27]). Feasibility analysis is carried out by propagating u^* through the dynamics given in Eq. (17) using a standard Runge–Kutta (RK) integrator. The candidate optimal control is deemed feasible if and only if the solution returned by the RK integrator coincides with the solution returned by the numerical solver to within a predefined tolerance (e.g., $\epsilon < 10^{-6}$, where ϵ is the error). All of the numerical solutions to problem ME presented in this paper have been verified against the necessary conditions and have been deemed feasible per the propagation test.

## III. Identifying the Mechanism for Energy Reduction

This section analyzes the minimum-energy solutions to the ME problem given in Eq. (17) for the case of minimum-time (off-eigenaxis) slews. The results, however, are also applicable to conventional eigenaxis maneuvering schemes.

A. Comparison with the Shortest-Time Maneuver

The shortest-time maneuver (STM) [10,11,31] is a time-optimal attitude maneuver determined as the solution to an optimal control problem. The STM maximizes the agility of a spacecraft by taking full advantage of the inertia ellipsoid [18], nonlinear rotational dynamics, and any operational constraints imposed system. To solve the STM, a problem formulation analogous to problem ME is employed with $J[x(\cdot), u(\cdot)(\cdot), t_f] = t_f$. For the same 180 deg z-axis
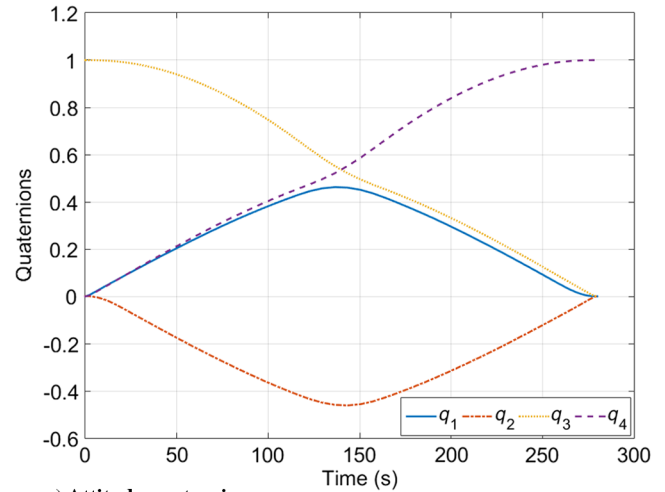

a) Attitude quaternions
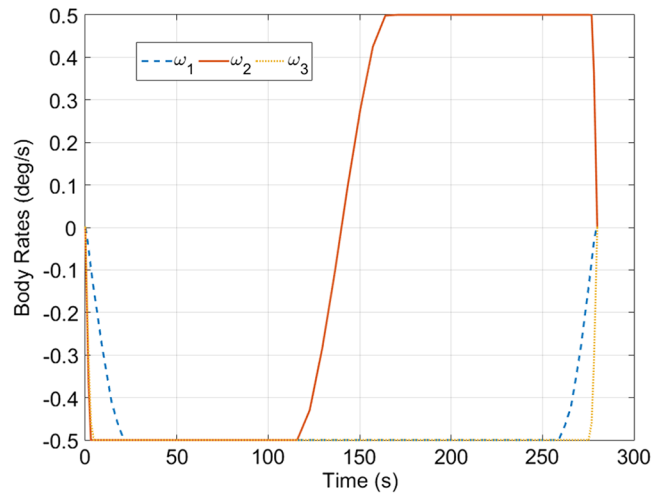
b) Spacecraft body rates
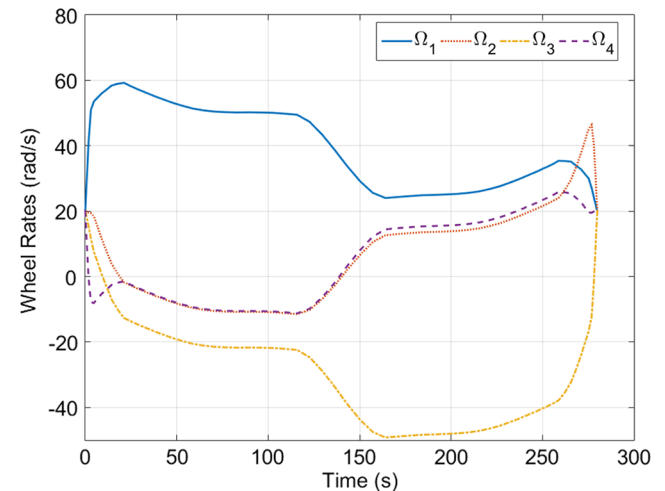
c) Reaction wheel speeds

Fig. 1 Minimum-energy solution for an agile attitude maneuver (a minimum-time maneuver).

slew example as in the previous section, we obtain the solution given in Fig. 3. Comparing the STM of Fig. 3 with the ME slew of Fig. 1, we note the following: 1) the spacecraft attitude and angular rate profiles have not changed; 2) the reaction wheel speed profiles have changed. The results illustrate what is obvious in retrospect. To effect the necessary momentum exchange with the spacecraft, the solution to the minimum-time maneuvering problem (Fig. 3) must admit a
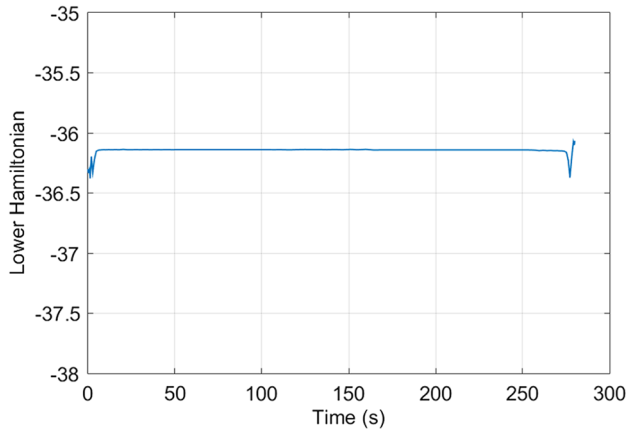
a) Hamiltonian evolution condition
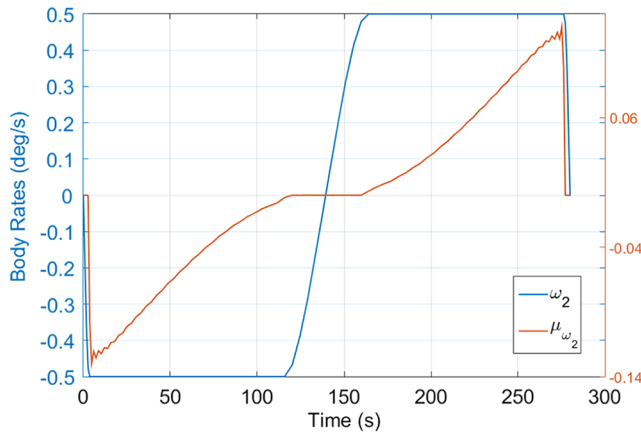

b) Complementarity condition

Fig. 2   Validation of example necessary conditions upon the solution to problem ME depicted in Fig. 1.

a) Attitude quaternions

b) Spacecraft body rates

c) Reaction wheel speeds

Fig. 3   Typical shortest-time attitude maneuver.

feasible reaction wheel speed profile. However, due to the additional degree(s) of freedom inherent to the redundant reaction wheel array, feasible reaction wheel speed profiles may not be unique. In particular, if the null space of reaction wheel projection matrix A is nontrivial, there exists an infinite number of feasible reaction wheel speed profiles for a given slew. Hence, for a given maneuver time, it is possible to reduce the energy consumed by searching the reaction wheel null space to eliminate losses associated with the original minimum-time solution by reallocating the control. This suggests that the relationship between the two different cost functionals that define the trade space of a redundant attitude control system is atypical. For example, conventional wisdom would suggest that reducing energy consumption would increase transfer time. However, in the case of a redundant attitude control system, it is in fact possible to reduce energy consumption without increasing the transfer time. Although an agile off-eigenaxis maneuver is considered here, it will be shown later that the same mechanism can be exploited for reducing the energy required to perform eigenaxis maneuvers.

The breakdown of the energy requirements for the maneuvers of Figs. 1 and 3 are summarized in Table 1. In Table 1, the cumulative electrical energy $\mathcal{E}^+$ is given along with the energy dissipated as heat $\mathcal{E}_{\text{total}}^{\text{loss}}$ and its two components of copper loss and friction loss. Although each maneuver has a transfer time of 279.9 s, the slews have significantly different energy requirements, as seen by the difference in the values of $\mathcal{E}^+$. By solving problem ME, it is possible to reduce the energy required by approximately 11%. The metrics in Table 1 show that solving the ME problem reduces the overall energy that is dissipated as heat, as seen by the copper loss and friction loss metrics, by approximately 11%. By marginally penalizing copper loss by 2%, the losses in overcoming wheel friction drag are substantially reduced, by 30%. Therefore, there exist less demanding shortest-time
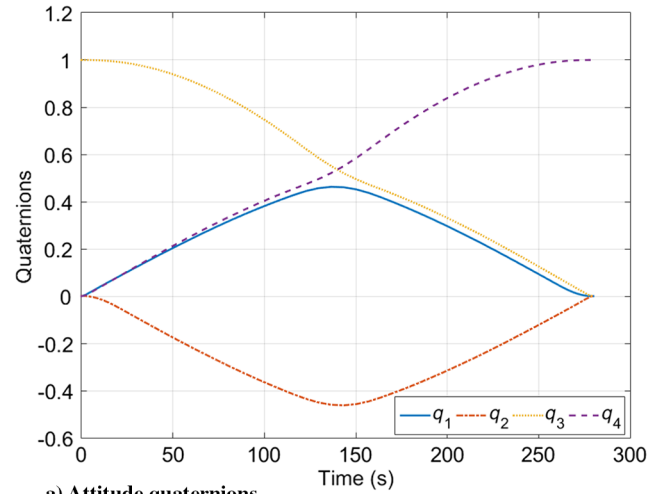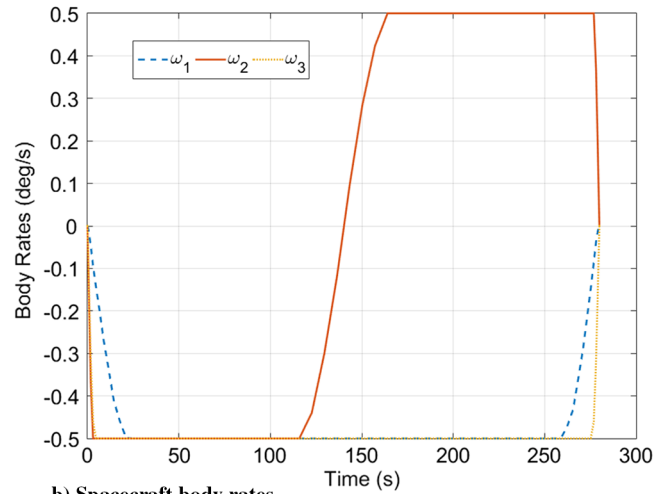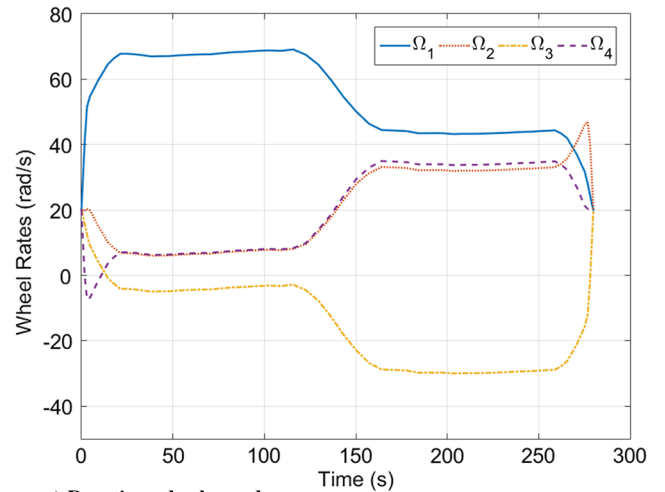
trajectories with respect to energy requirements as well as amount of generated dissipative losses.

B.   Exploiting the Null Space to Reduce Energy Requirements

In this section, we further explore the utility of the reaction wheel null space and develop a simplified problem that facilitates real-time implementation of (sub)optimal null space solutions for reducing energy requirements. Let $\{q_{\text{ref}}(t), \omega_{\text{ref}}(t), \Omega_{\text{ref}}(t), \tau_{\text{ref}}(t)\}, t \in [0, t_f]$ be an arbitrary feasible reference state-control profile that satisfies the

Table 1   Energy metrics for a baseline shortest-time maneuver and a minimum-energy maneuver equivalent in transfer time[a]

Maneuver type	$\mathcal{E}^+$, J	$\mathcal{E}_{\text{total}}^{\text{loss}}$, J	C_{loss}, J	$\mathcal{F}_{\text{loss}}$, J
Shortest-time maneuver	162.0	136.3	79.7	56.6
ME shortest-time maneuver	143.9 (−11.2%)	121.0 (−11.2%)	81.3 (+1.9%)	39.7 (−29.8%)

[a]Values in parenthesis represent percentage change from baseline.

dynamics, boundary conditions, and constraints given in Eq. (17). By exploring null motion explicitly, we will show in the following that the energy consumption of any given feasible solution can be improved without changing the reference quaternion $q_{\text{ref}}(t)$ or the body rate $\omega_{\text{ref}}(t)$ profile.

For the tetrahedron wheel configuration with projection matrix A given in Table A1, it is straightforward to show that

$$\text{null}(A) = \text{span}\{[1, 1, 1, 1]^T\} \subset \mathbb{R}^4$$

Consider a modification on the reference control τ_{ref} in the null space of matrix A

$$\tau(t) = \tau_{\text{ref}}(t) + \delta\tau(t) \cdot [1, 1, 1, 1]^T$$

where $\delta\tau(t):[0, t_f] \to \mathbb{R}$ is an augmentation factor to the reference control through null motions. From the dynamics, it is easy to show that the modified control $\tau(t)$ produces the same quaternion $q_{\text{ref}}(t)$ and the body rate $\omega_{\text{ref}}(t)$ as the reference feasible trajectory. Similarly, the effect of the modified control on the wheel speed is given by

$$\Omega(t) - \Omega_{\text{ref}}(t) = \int_0^t \delta\tau(s)\, ds \cdot J_{\text{rw}}^{-1}[1, 1, 1, 1]^T$$

For simplicity in exposition, we assume all reaction wheels are identical, therefore $J_{\text{rw}}^{-1} = cI \in \mathbb{R}^{N_{\text{rw}} \times N_{\text{rw}}}$, where $c \in \mathbb{R}_{>0}$ is the multiplicative inverse of the inertia of a reaction wheel. (If wheels are not identical, so that J_{rw} is not a multiple of the identity matrix, the following analysis can be easily adapted.) It follows that $\Omega(t) = \Omega_{\text{ref}}(t) + \delta\Omega(t) \cdot [1, 1, 1, 1]^T$, where $\delta\Omega$ is a one-dimensional function satisfying

$$\dot{\delta\Omega} = c \cdot \delta\tau \tag{19}$$

Because each wheel is assumed to begin and end with the same angular velocity, a practical operational constraint is given by the boundary conditions in Eq. (17), and so $\delta\Omega$ must have

$$\delta\Omega(0) = \delta\Omega(t_f) = 0 \tag{20}$$

Now it is clear that any function pair $(\delta\Omega(t), \delta\tau(t))$ that simultaneously satisfies the one-dimensional linear dynamics in Eq. (19), boundary condition (20), and constraints

$$|\Omega_{\text{ref},i} + \delta\Omega| \leq \Omega_{\max},$$
$$|\tau_{\text{ref},i} + \delta\tau| \leq \tau_{\max}, \qquad i = 1, 2, \ldots, N_{\text{rw}} \tag{21}$$

produces a trajectory $\{q_{\text{ref}}(t), \omega_{\text{ref}}(t), \Omega(t), \tau(t)\}$ that satisfies all the constraints of the minimum-energy optimal control problem given in Eq. (17). After some straightforward derivations, the energy consumption along such feasible solutions, generated through null motions, is given by

$$J = \frac{R}{K_T^2} \sum_{i=1}^{N_{\text{rw}}} \int_0^{t_f} [\delta\tau(t) + \tau_{\text{ref},i}(t)]^2 + k[\delta\Omega(t) + \Omega_{\text{ref},i}(t)]^2 \, dt \tag{22}$$

where $k = \beta^2 + \beta K_T^2/R$.

Based on this observation, it is possible to start from any given feasible solution of Eq. (17) (e.g., shortest-time maneuvers) and seek a function pair $(\delta\Omega(t), \delta\tau(t))$ to minimize the energy Eq. (22), without changing the spacecraft attitude and body rate trajectories. The function pair $(\delta\Omega(t), \delta\tau(t))$ can be determined by the following optimal control formulation, hereafter referred to as the null motion (NM) problem:

$$(\text{NM}) \begin{cases} \text{State:} & \delta\Omega \in \mathbb{R}, \text{Control:} \delta\tau \in \mathbb{R} \\ \text{Minimize:} & J[\delta\Omega(\cdot), \delta\tau(\cdot)] = \frac{R}{K_T^2} \sum_{i=1}^{N_{\text{rw}}} \int_0^{t_f} [\delta\tau(t) + \tau_{\text{ref},i}(t)]^2 + k[\delta\Omega(t) + \Omega_{\text{ref},i}(t)]^2 \, dt \\ \text{Subject to:} & \dot{\delta\Omega} = c\delta\tau, \delta\Omega(0) = \delta\Omega(t_f) = 0 \\ & |\Omega_{\text{ref},i}(t) + \delta\Omega(t)| \leq \Omega_{\max}, \\ & |\tau_{\text{ref},i}(t) + \delta\tau(t)| \leq \tau_{\max}, i = 1, 2, \ldots, N_{\text{rw}} \end{cases} \tag{23}$$

The solution to problem NM generates a motion in the null space of the projection matrix A so that the feasibility of the system state trajectories are maintained, while the overall energy consumption is reduced.

It is important to point out that problem NM can be solved with extreme efficiency due to the quadratic cost function and one-dimensional linear dynamics. Indeed, when the wheel speed and torque constraints (21) are not active, problem NM admits an analytic solution given as

$$\delta\Omega(t) = \left(\frac{\Omega_b}{e^{c\sqrt{k}t_f} - e^{-c\sqrt{k}t_f}}\right)\left(e^{c\sqrt{k}t}\left(1 - e^{-c\sqrt{k}t_f}\right)\right.$$
$$\left. + e^{-c\sqrt{k}t}\left(e^{c\sqrt{k}t_f} - 1\right)\right) - \frac{1}{N_{\text{rw}}} \sum_{i=1}^{N_{\text{rw}}} \Omega_{\text{ref},i}(t) \tag{24}$$

$$\delta\tau(t) = -\left(\frac{\sqrt{k}\Omega_b}{e^{c\sqrt{k}t_f} - e^{-c\sqrt{k}t_f}}\right)\left(e^{c\sqrt{k}t}\left(e^{-c\sqrt{k}t_f} - 1\right)\right.$$
$$\left. + e^{-c\sqrt{k}t}\left(e^{c\sqrt{k}t_f} - 1\right)\right) - \frac{1}{N_{\text{rw}}} \sum_{i=1}^{N_{\text{rw}}} \tau_{\text{ref},i}(t) \tag{25}$$

We note that, for a simulation study of the spacecraft parameters given in the Appendix, in which several hundreds of simulations with various boundary conditions and transfer times were performed, wheel speed saturations were not observed and that motor torque saturation only occurred when the slew time was within 0.5% of t_{STM}. The former is very reasonable for many practical systems in which a portion of the reaction wheel momentum envelope is reserved to accommodate momentum accumulation. Hence, Eqs. (24) and (25) provide essentially a closed-form solution to problem NM. In the rare instances where the wheel speed and/or torque constraints are active,

Table 2 Equivalency between minimum-energy formulation and null motion formulation for a 180 deg z-axis slew with $T = 281.8$ s

Maneuver type	$\mathcal{E}^+$, J	$\mathcal{E}_{\text{total}}^{\text{loss}}$, J	$\mathcal{C}_{\text{loss}}$, J	$\mathcal{F}_{\text{loss}}$, J
Feasible maneuver to problem ME	133.9	105.8	50.2	55.6
Problem ME solution	114.5	90.8	52.2	38.6
Problem NM solution	114.6	90.9	52.3	38.6

an analytic solution to problem NM can be complicated to derive; however, a numerical solution to this one-dimensional linear quadratic problem is easy to generate in real time onboard the spacecraft.

As a demonstrative example, consider the same 180 deg rotation about the spacecraft z-body axis as before. In this case, the transfer time is set to be $T = 281.8$ s, slightly longer than the minimum-time solution ($t_{\text{STM}} = 279.9$). Three feasible maneuvers are generated and compared: 1) a feasible fixed-time maneuver; 2) a minimum-energy maneuver obtained by solving problem ME per Eq. (17); and 3) a null motion solution based on Eqs. (24) and (25) where the feasible reference trajectory ($\Omega_{\text{ref}}, \tau_{\text{ref}}$) is the same as in maneuver 1.

Table 2 compares the energy metrics for these three maneuvers. It can be seen that both the ME and NM maneuvers perform nearly equivalently in terms of energy consumption. Although the ME formulation reduces energy requirements by coordinating the reaction wheel null motions while shaping the angular velocity body profile of the spacecraft, the solution to problem NM also develops a highly efficient solution. This result is in spite of the fact that the minimization in problem NM is agnostic to the satellite attitude and rate profile and is performed only over the space of null motions.

The null motion analysis presented in this section enables a few interesting applications, two of which are summarized as follows:

1) The null motion formulation (23) and its analytic solution (24) and (25) provide a fast and computationally inexpensive way to refine any given feasible trajectory for energy reduction, thus generating suboptimal minimum-energy maneuvers, considered suboptimal because the energy reductions are obtained by considering only a subset of the state space. Such substantial efficiency in solving problem NM is a very attractive feature for real-time implementation.

2) Problem NM provides a new means of verification and validation that is both computationally inexpensive and easily identifiable. Consider a candidate solution $\{q^*, \omega^*, \Omega^*, \tau^*\}$ to the ME problem. We can take this candidate solution as the reference in the NM problem. If $\{q^*, \omega^*, \Omega^*, \tau^*\}$ is the true minimum-energy maneuver, the solution to problem NM should not admit additional energy reduction (i.e., the cost of problem NM should be the same as the cost of the ME formulation). Independent to Pontryagin's minimum principle, the null motion formulation (23) provides an alternative way for verifying the optimality of the minimum-energy solution.

To illustrate the second point, consider an ME slew with $T = 307$ s, which will be seen in the next section to be the transfer time that balances both transfer time and energy. Figure 4a shows that the solution to the NM problem gives $\delta\tau(t) \equiv 0$. Furthermore, the reaction wheel angular velocities are identical for both problem formulations (see Fig. 4b). The NM solution therefore indicates that energy cannot be further reduced from the ME solution by performing null motions, a condition that a minimum-energy maneuver must satisfy.
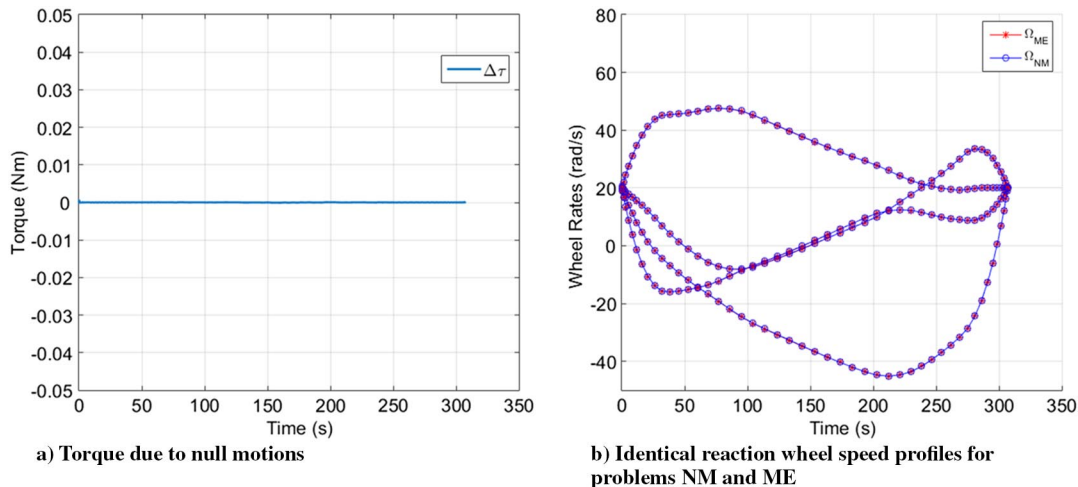
IV. Relationship Between Transfer Time and Minimum Energy

The purpose of this section is to study the relationship between transfer time and energy required to perform a slew for both eigenaxis and off-eigenaxis maneuvering. By identifying the energy/time relationships, the shortest-time maneuver satisfying a given energy budget may be identified, and a comparison may be made between on- and off-eigenaxis maneuvering concerning energy and transfer time. In determining the relationship, a 180 deg slew about the spacecraft's z-body axis is first considered, whose initial and final quaternions are $q^0 = [0, 0, 1, 0]^T$ and $q^f = [0, 0, 0, 1]^T$. Extensive simulations (over several hundreds) in which initial and final attitude were varied, confirmed that the relationship identified between energy and time presented for this 180 deg slew are indicative of the results for other slew sizes. The run time to generate simulation results for each set of boundary conditions ranged from 10 s up to about 2 min, with the average run time of approximately 55 s. We note that, because maneuvers are often planned a priori, the solution times are amenable to practical generation.

Following the single-slew analysis, the energy and transfer time relationship is analyzed in a typical setting for an imaging satellite: a multipoint maneuver consisting of a sequence of five slews. The multislew analysis demonstrates that the energy/time relationship identified for the 180 deg canonical maneuver holds under varying slew size, as well as path.

A. Off-Eigenaxis Slew Analysis

The shortest-time maneuver from Sec. II provides the lower time bound t_{STM} for which the rest-to-rest slew may be performed. By solving a series of ME formulation (off-eigenaxis) of fixed times $T \geq t_{\text{STM}}$, a Pareto front may be generated to show the minimum energy required to perform the slew for a given transfer time. This Pareto front for off-eigenaxis maneuvering is given in Fig. 5, with the minimized cost $\mathcal{E}_{\text{total}}^{\text{loss}}$ shown as the lower curve with square markers that indicate the particular slew times solved. Recall the cost functional $\mathcal{E}_{\text{total}}^{\text{loss}}$ in problem ME measures the cumulative dissipative losses incurred over a slew. From a solution to problem ME, the actual energy consumption $\mathcal{E}^+$ may be calculated a posteriori and is given by the top-most curve with asterisk markers in Fig. 5. We note that the

a) Torque due to null motions

b) Identical reaction wheel speed profiles for problems NM and ME

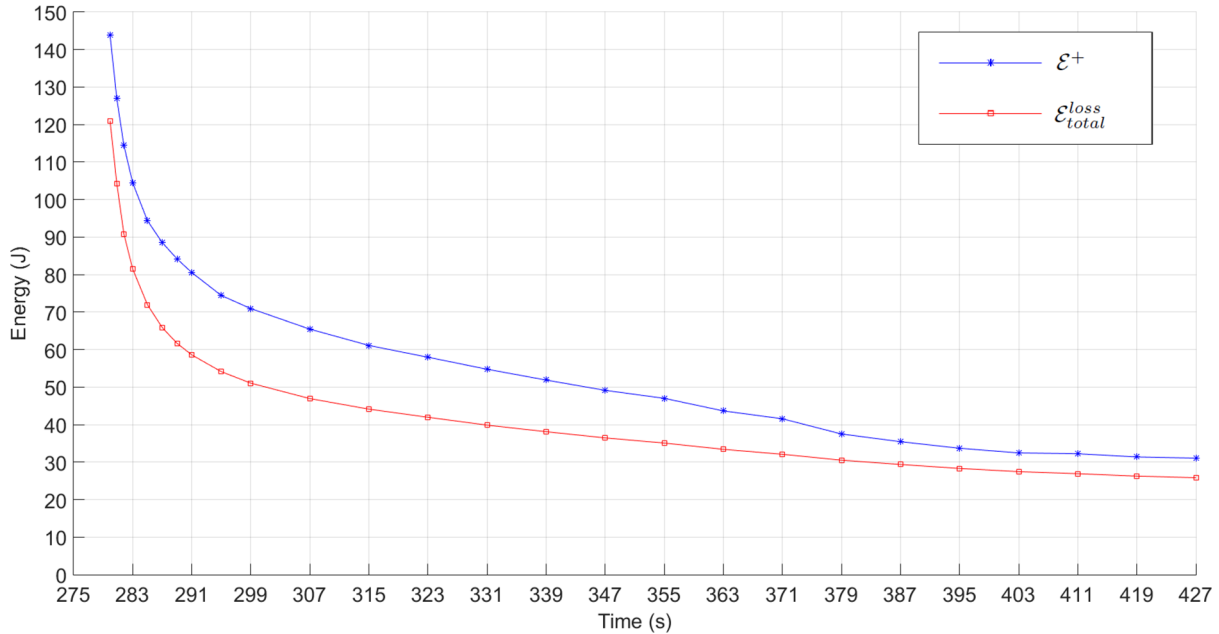**Fig. 4 Solution to problem NM for an ME reference maneuver with a transfer time of 307 s.**

Fig. 5 Pareto fronts to the 180 deg z-body axis for minimum-energy off-eigenaxis maneuvering.

optimal cost $\mathcal{E}_{\text{total}}^{\text{loss}}$ is always slightly smaller than the actual consumed energy $\mathcal{E}^+$ and forms a lower bounding curve. That the proxy $\mathcal{E}_{\text{total}}^{\text{loss}}$ forms a lower bounding curve is consistent with the fact that the control applied is optimal with respect to minimizing dissipative losses $\mathcal{E}_{\text{total}}^{\text{loss}}$, but in general is nonoptimal with respect to $\mathcal{E}^+$.

With the aid of the visualization provided by the Pareto front in Fig. 5, the nonlinear relationship between the transfer time and the minimum energy required to perform the slew is observed to consist of three phases when considering time as increasing from the shortest time. First, as transfer time is increased from the shortest time, there exists a time window in which the energy required to perform the maneuver drastically decreases at a fast rate. Denoting this portion of the Pareto front as the head, this window of asymptotic decay beyond the shortest time may be identified with the time interval [t_{STM}, 307]. Second, the relationship in Fig. 5 showcases that there exists a point in time where further increasing transfer time results in insignificant reductions in energy. Defining this portion of the Pareto front as the tail, this time window may be defined as the interval [395, ∞). Finally, a third portion of the Pareto front may be identified simply as the region in between the head and tail of the Pareto front [307, 395] and depicts that energy decays roughly proportionally to increasing transfer times.

The behavior of energy with respect to time within the head portion of the Pareto front validates the intuition that shortest-time maneuvers can indeed be costly maneuvers with respect to energy. More notably though, the head of the Pareto front signifies that small increases in transfer time from the shortest time net significant savings in energy. In other words, there exists near-time-optimal maneuvers that cost much less than their minimum-energy shortest-time maneuver counterpart. Thus, it is possible to balance energy and transfer time requirements when missions demand an agile setting, despite intuitive notions to the contrary.

The tail portion of the Pareto front in Fig. 5 is inversely analogous to the head region. Whereas small increases in transfer time near t_{STM} net substantial savings in energy in the head region, increases in transfer time within the tail portion of the Pareto front net only minor savings in energy. Although the Pareto front of Fig. 5 stops with a transfer time of 427 s, the energy and time relationship in the tail section continues in like manner for all time, slowly decaying over large intervals of time. Therefore, in a setting where transfer time is of no concern, the tail portion of the energy/time relationship depicts that there is not much benefit from significantly increasing the transfer time of a maneuver with respect to energy consumption.

B. Minimum-Energy Eigenaxis Slew Analysis

With the ME-EAM formulation along with the shortest-time EAM, a Pareto front describing the minimum-energy transfer time relationship with respect to eigenaxis maneuvering may be built analogously to the Pareto front constructed in Sec. IV.A. The result of this construction is given in Fig. 6 and has been superimposed upon the off-eigenaxis Pareto front of Fig. 5 to facilitate comparison. For each of the curves in Fig. 6, the minimum energy is reported as the $\mathcal{E}^+$ metric.

The minimum-energy EAM Pareto front shown in Fig. 6 (denoted with triangle markers that indicate the particular slew times solved) depicts an analogous relationship with respect to energy and transfer time compared with the off-eigenaxis Pareto front. Namely, near the shortest time (for an eigenaxis maneuver), energy costs significantly increase, showing that there exist eigenaxis maneuvers with a near time-optimal transfer time that require significantly less energy to execute. More interestingly, Fig. 6 clearly shows that the minimum-energy EAM curve lies completely encompassed within the region defined by the off-eigenaxis curve for all transfer times. Both maneuver types are analogous with respect to energy for slew times $T \geq 395$ s. This coincide point depicts that there exists a point in transfer time in which on- and off-eigenaxis maneuver types are equivalent with respect to energy consumption. In other words, when the transfer time is sufficiently large, expanding the solution space from eigenaxis to noneigenaxis slews provides no benefit in energy saving. For sufficiently large transfer times, the minimum-energy slew is an eigenaxis maneuver.

From the time-optimal transfer time t_{STM} of 279.9 s to the coincide point of 395 s, the two Pareto fronts in Fig. 6 imply the existence of a trade space between transfer time, as well as energy between eigenaxis and off-eigenaxis maneuvering. A geometric argument may be made in discerning a tradeoff between the two maneuver types: A given energy budget may be visualized with a horizontal line in Fig. 7, and in like manner, a time budget may be visualized as a vertical line as illustrated in Fig. 8.

Figure 7 explores the trade space with respect to transfer time between eigenaxis and off-eigenaxis maneuvers. The horizontal lines in Fig. 7 depict that, for every minimum-energy eigenaxis slew, there exists an energy equivalent off-eigenaxis maneuver with a smaller transfer time. Additionally, each of these off-eigenaxis maneuvers incur less dissipative losses. The extreme case with respect to transfer time is identified in Fig. 7 by the maneuver that is energy equivalent to the minimum-energy shortest-time eigenaxis maneuver, which is
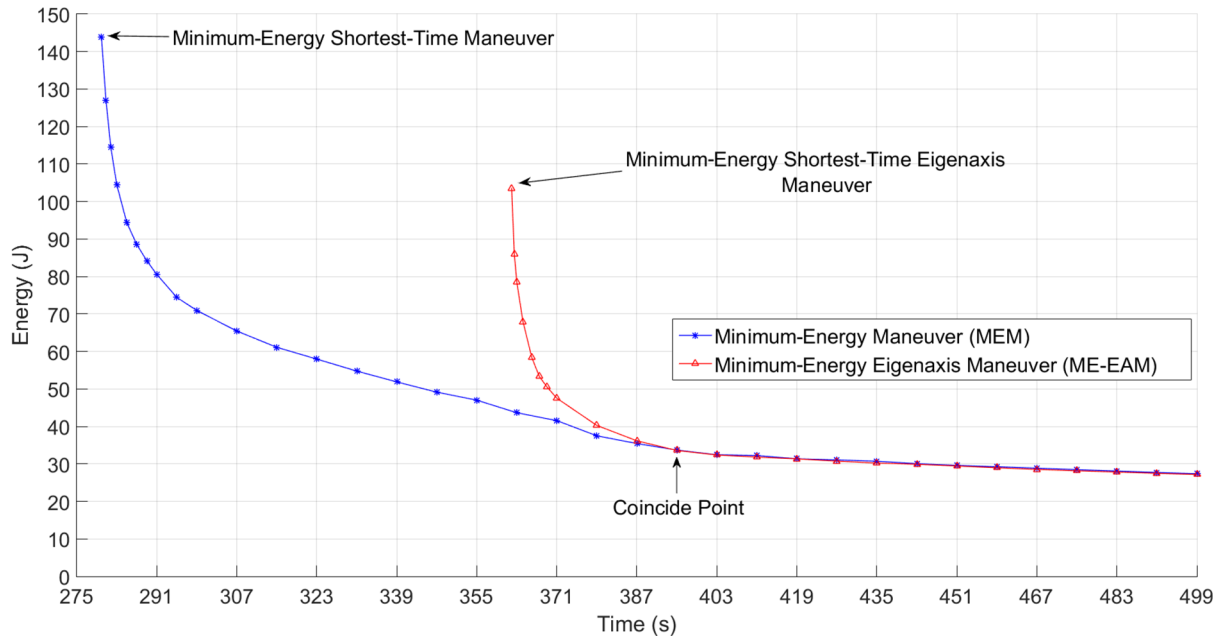
Fig. 6   Pareto fronts for minimum-energy off-eigenaxis and minimum-energy eigenaxis maneuvering for a 180 deg z-body-axis slew; energy reported as $\mathcal{E}^+$.
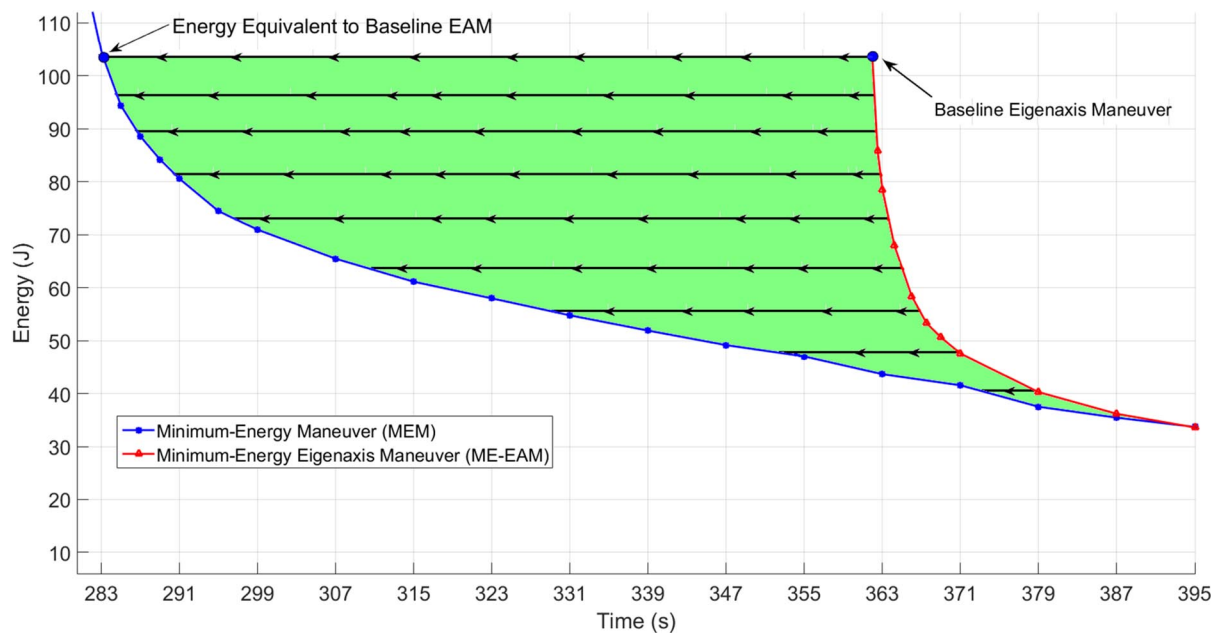

Fig. 7   Trade space depicting the benefit of off-eigenaxis maneuvers, compared with eigenaxis, with respect to energy.

hereafter referred to as the "baseline EAM." Compared with the baseline EAM, by allowing off-eigenaxis maneuvering, it is possible to decrease the transfer time by 21.7% (from 362.0 to 283.1 s) without consuming any more energy than the baseline eigenaxis maneuver (103.5 J), while simultaneously incurring 12% less dissipative losses. Table 3 summarizes the energy metrics and transfer time (TT) for the baseline eigenaxis maneuver and off-eigenaxis the energy-equivalent maneuver. Comparing this agile maneuver to time-optimal (shortest-time) maneuvering, for the same energy budget of the baseline eigenaxis maneuver, the transfer time may be brought within 1% of t_{STM} by maneuvering off-eigenaxis while reducing the standard STM energy by 36.1% and reducing dissipative losses by 40.6%.

Therefore, the transfer time may be substantially reduced by control reallocation while simultaneously decreasing the amount of dissipative losses incurred to perform an agile maneuver, without

exceeding the energy budget of a canonical EAM. Additionally, with respect to shortest-time maneuvering, for a negligible increase in transfer time, the large effort associated with time-optimal maneuvering may be substantially decreased by opting for a near-time-optimal maneuver. Synthesizing the analysis of these three maneuvers, along with the energy/time spectrum in Fig. 6, it is apparent that there exist desirable agile maneuvering capabilities within (minimum) energy budgets of industry standard eigenaxis maneuvering.

Next, we turn our attention to the trade space of energy with respect to transfer times of minimum-energy eigenaxis maneuvering: Fig. 8 depicts that, in the case where EAM transfer times are acceptable to meet mission requirements, the energy can be substantially reduced from even minimum-energy EAMs by control reallocation and maneuvering off-eigenaxis. The extreme case identified in the trade
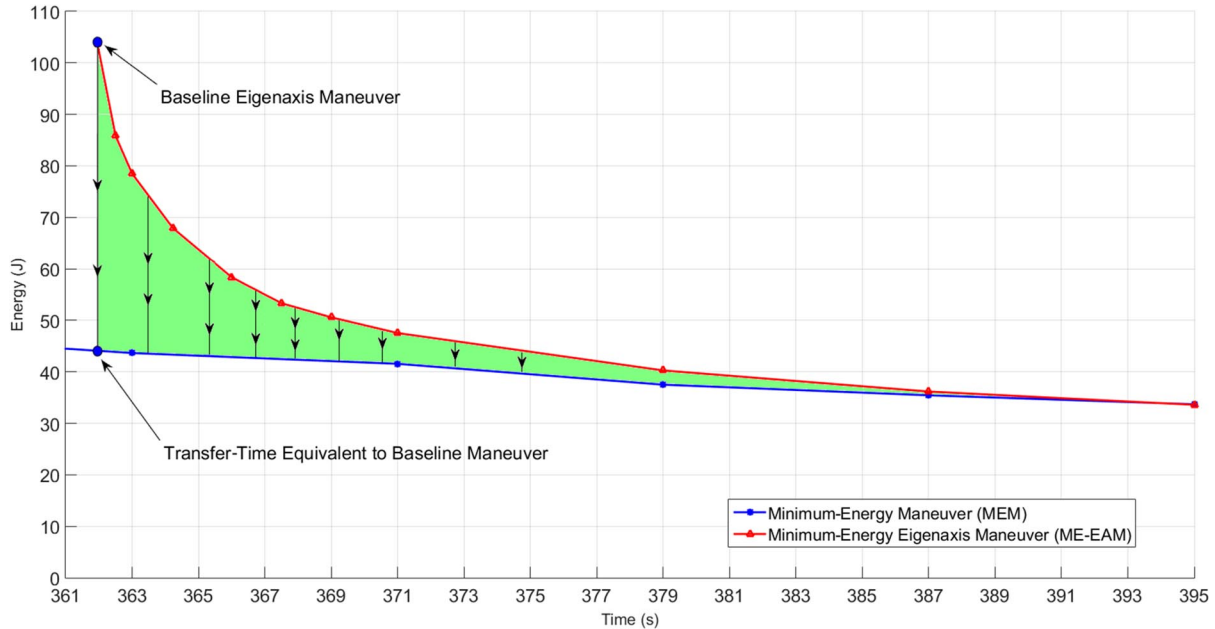
Fig. 8   Trade space depicting the benefit of off-eigenaxis maneuvers, compared with eigenaxis, regarding transfer time.

space of Fig. 8 is the off-eigenaxis maneuver, which completes in the same transfer time as the baseline eigenaxis maneuver. For the same transfer time as the baseline eigenaxis maneuver (which completes in 362.0 s), by maneuvering off-eigenaxis, the energy (given by $\mathcal{E}^+$) required to perform the baseline EAM is reduced by 57.5% (from 103.5 to 44.0 J), and the cumulative dissipative losses incurred by performing the ME-EAM are reduced by 63.2% (from 91.4 to 33.6 J). Comparing the individual dissipative losses between the two maneuvers, although the off-eigenaxis maneuver incurs 10% more friction loss (22.9 to 25.1), it is able to reduce the copper loss by 87% (from 68.5 to 8.6 J). The considerable reduction in dissipative losses (from 68.5 to 33.6 J), and therefore less heat to reject, is due to the substantial reduction in copper loss.

The large amount of copper loss incurred by the baseline EAM is due to the torque demand required to maintain the motion along the eigenaxis. By being able to maneuver off-eigenaxis, the transfer-time equivalent maneuver is able to exploit the inertia properties of the spacecraft under both the nonlinear dynamics and constraints, requiring much less torque authority, and hence considerably less copper loss. Therefore, by maneuvering the spacecraft off-eigenaxis, energy and dissipative losses may be substantially reduced when compared with conventional eigenaxis maneuvering.

Shown in Fig. 9 are the y-axis boresight traces for on- and off-eigenaxis maneuvers for the 180 deg z-body-axis slew. As expected, the eigenaxis maneuver traces out the shortest angular path, as represented by the straight-line path between the two orientations. Similarly, the boresight traces of the two maneuvers equivalent to the baseline eigenaxis maneuver each illustrate off-eigenaxis motion, as seen by deviating from the circular arc traced by the baseline EAM.

C.   Operational Scenario

This section expands upon the analysis of the previous sections, by considering a multipoint slew consisting of five sequential maneuvers. A multislew maneuver is considered here to demonstrate that each of the properties resultant from the analysis of the single

slew directly translate to a typical operational scenario for an imaging spacecraft involving multiple collection points. The five-point multislew is based off of the STAR pattern developed in [11] and consists of reorienting the imaging boresight (aligned with the spacecraft y axis) over both medium angle ($\approx$30 deg) and large angle ($\gg$30 deg) slews. The relevant attitude parameters for both on- and off-eigenaxis maneuvering for the five-point multislew are given in Table 4.

Four maneuver types are selected to explore the trade space between energy and transfer time between on- and off-eigenaxis maneuvering: 1, 2) the ME shortest-time maneuver and ME shortest-time eigenaxis maneuver, which represent the minimum energy required to complete the multislew for time-optimal off- and on-eigenaxis maneuvers, respectfully, referred to as the "baseline off-eigenaxis maneuver" and "baseline eigenaxis maneuver"; 3) the (off-eigenaxis) maneuvers, which are energy equivalent (with respect to $\mathcal{E}^+$) to each baseline eigenaxis maneuver; and 4) the (off-eigenaxis) maneuvers, which are equivalent with respect to transfer times of the baseline eigenaxis maneuver. Figure 10 depicts each of the four maneuver types as corner points on the energy-time trade space for a conceptualized Pareto front.

For the multislew, the ME shortest-time maneuvers, compared with their time-optimal EAM counterparts (the baseline EAMs), are

Table 4   Sequence of quaternions for the five-point multislew maneuver

Orientation	q_1	q_2	q_3	q_4
1	0.0602	0.1850	0.6165	0.7629
2	0.2860	0.0069	0.5607	0.7770
3	0.1864	0.0045	0.0854	0.9788
4	0.1195	0.1431	0.7921	0.5812
5	0.1314	0.1263	0.2458	0.9520
6	0.1693	0.0781	0.4666	0.8646

Table 3   Metrics to the minimum-energy shortest-time eigenaxis maneuver (baseline EAM) and energy equivalent off-eigenaxis maneuver[a]

Maneuver type	TT, s	$\mathcal{E}^+_{\text{elec}}$, J	$\mathcal{E}^{\text{loss}}_{\text{total}}$, J	$\mathcal{C}_{\text{loss}}$, J	$\mathcal{F}_{\text{loss}}$, J
Baseline EAM	362.0	103.5	91.4	68.5	22.9
Energy equivalent to baseline EAM	283.1 (−21.7%)	103.5 (0.0%)	80.8 (−11.6%)	42.7 (−37.7%)	38.2 (+66.8%)

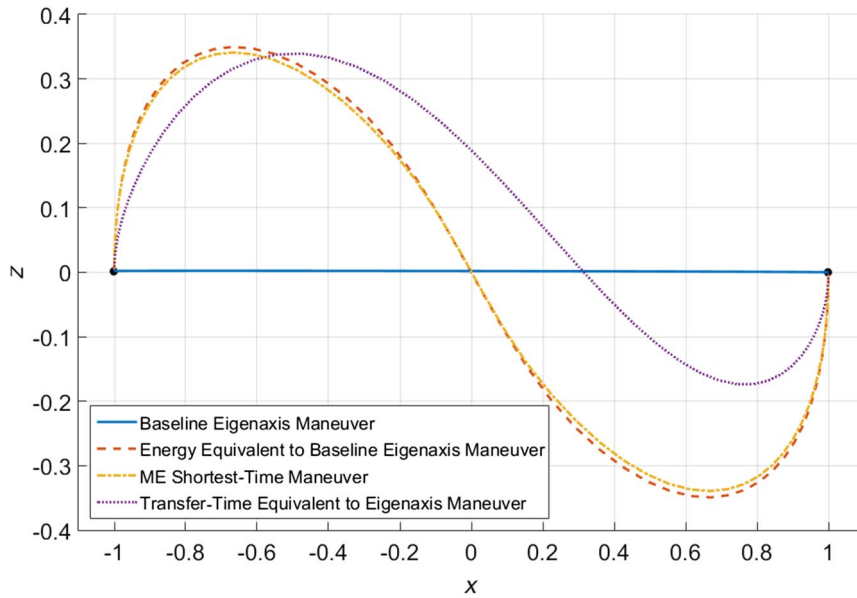[a]Values in parenthesis represent percentage change from baseline EAM.

Fig. 9   Boresight traces for various maneuver types performing a 180 deg z-body-axis slew.
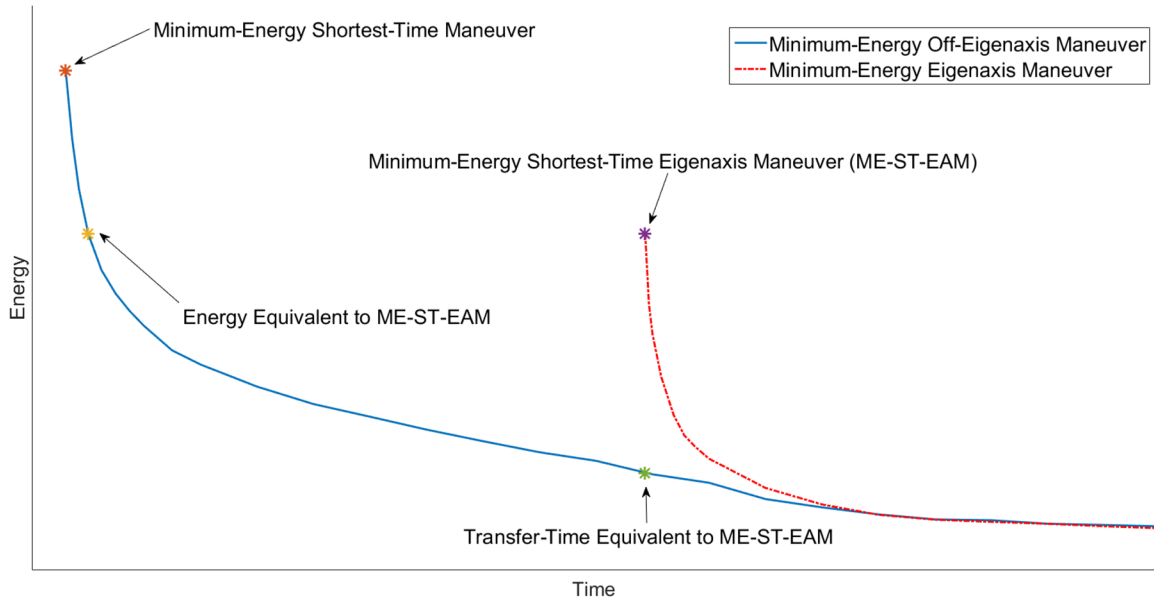

Fig. 10   Visualization of the four maneuver types to explore the trade space between on- and off-eigenaxis maneuvering for the multislew scenario.

able to decrease transfer time by 19.6% (from 649.4 to 522.0 s) but at the substantial cost of increased energy consumption, up by 124% (from 409.6 to 918.5 J). It seems that experience and intuition is true, that minimum-time solutions demand considerable effort, but because each individual slew has an energy and transfer time relationship analogous to Fig. 6, there exist agile maneuvers (i.e., maneuvers with a smaller transfer time than eigenaxis maneuvering) with significantly less stringent energy requirements. By maneuvering off-eigenaxis, for the same energy budget as the baseline EAMs, the multislew may be completed within 5.7% of the

time-optimal transfer time (from 522.0 to 551.9 s) while consuming 55.6% less energy than the baseline off-EAMs (from 918.5 to 408.6 J). Comparing this agile maneuver, the transfer time of the baseline EAMs may be reduced by 15% (from 649.4 to 551.9 s) for the same energy required to perform canonical eigenaxis maneuvering. Considering the situation of minimizing energy by allowing off-eigenaxis maneuvering, the maneuver-set transfer-time equivalent to the baseline EAMs is able to decrease the energy requirements by 53% (from 409.6 to 191.4 J), the lowest of the four maneuver types. Table 5 summarizes the tradeoffs between energy

Table 5   Difference in energy and time by opting between various maneuver types for the multipoint slew

| Change of maneuver type	%Δ TT	%Δ$\mathcal{E}_{\text{elec}}^{+}$
Baseline eigenaxis maneuver → ME shortest-time maneuver	−19.6%	+124.2%
ME shortest-time maneuver → Energy equivalent eigenaxis maneuver	+5.7%	−55.5%
Baseline eigenaxis maneuver → Energy equivalent eigenaxis maneuver	−15.0%	−0.2%
Baseline eigenaxis maneuver → Transfer-time equivalent eigenaxis maneuver	0%	−53.3%
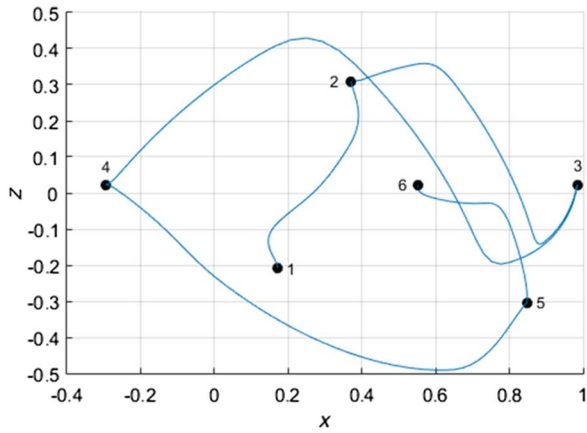
a) Minimum-Energy Shortest-Time Maneuver
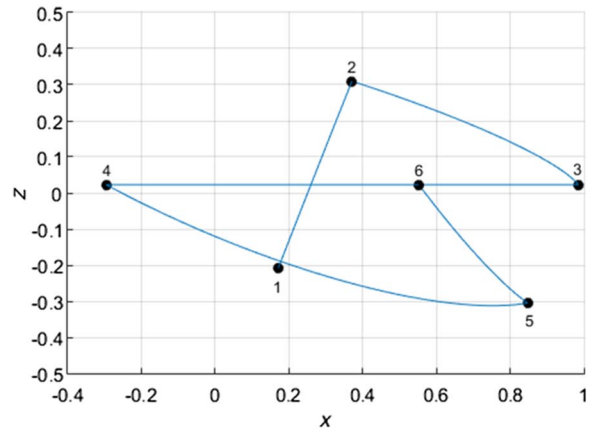
b) Minimum-Energy Shortest-Time Eigenaxis Maneuver

Fig. 11 Boresight traces to two of the four maneuver types from Fig. 10.
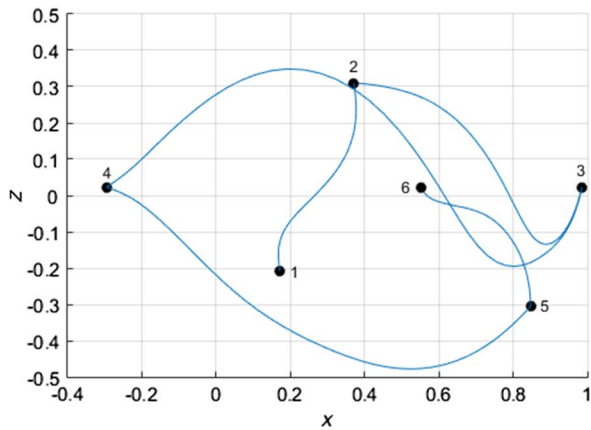
a) Energy Equivalent to Minimum-Energy
Shortest-Time Eigenaxis Maneuver
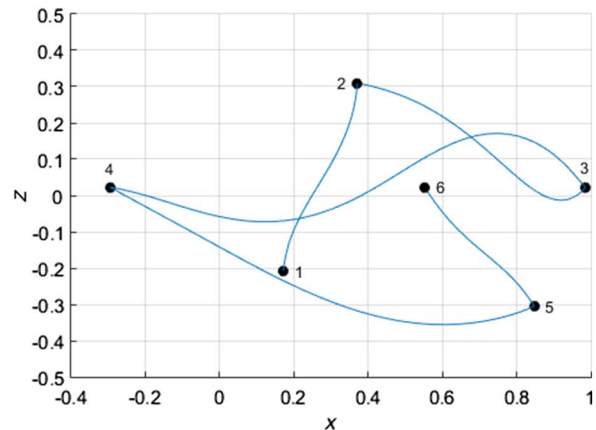
b) Transfer-Time Equivalent to Minimum-Energy
Shortest-Time Eigenaxis Maneuver

Fig. 12 Boresight traces to two of the four maneuver types from Fig. 10.

and transfer time for various maneuver types. Viewing the four representative maneuver types together, the energy equivalent and transfer-time equivalent off-eigenaxis maneuvers, compared with the baseline EAMs, depict that there exists a significant penalty in slew time and energy when enforcing eigenaxis rotations. Similarly demonstrated by this simulation example is that the properties inherent to the single slew analysis translate to a multislew environment. By allowing the spacecraft to maneuver off-eigenaxis, the optimization may take full advantage of the attitude control capability as represented by the spacecraft agilitoid [18], as seen by the energy and transfer-time equivalent maneuvers to the baseline eigenaxis maneuver.

The boresight traces over the course of the five-point multislew are given in Fig. 11 for the baseline off- and on-EAMs, along with the energy equivalent and transfer-time equivalent maneuvers in Fig. 12. The imaging boresight for the baseline EAMs, as expected, traces out shortest circular arcs between the five capture locations. Similarly expected, from Fig. 11a, the motion of the boresight to the baseline off-EAMs deviates from the eigenaxis for each of the five orientations. For reference, the boresight trace to the standard STMs are identical to those given in Fig. 11a. Similarly, the energy equivalent and transfer-time equivalent maneuvers show that the entire multipoint slew is performed off-eigenaxis. That the traced path between each of the five orientations for the three off-eigenaxis maneuver types are each distinct is due to the combination of the boundary conditions as well as the inertia properties of the spacecraft. Because the rotational maneuvers are not restricted about an eigenaxis, the optimization may minimize energy by taking full

advantage of the spacecraft's geometry per the boundary conditions when determining a feasible slew.

V. Conclusions

This paper has identified and studied the nonlinear relationship that arises between slew time and energy for reaction wheel attitude control under both conventional eigenaxis and agile off-eigenaxis maneuver schemes. The nonlinear time/energy relationship showed two main results that hold both for eigenaxis and noneigenaxis maneuvers: 1) There exist a continuum of near-time-optimal maneuvers that require substantially less energy than their shortest-time counterpart. The saving in energy is realized via a reallocation of the control effort by exploiting energy-reducing null motions within the control space while shaping the velocity of the spacecraft body. 2) There exists a slew time beyond which savings in energy become negligible.

This paper further demonstrates the existence of a trade space between on- and off-eigenaxis maneuvering. This trade space shows that a significant penalty is incurred upon slew time and energy when enforcing eigenaxis maneuvering: 1) By maneuvering off-eigenaxis, slew time may be significantly decreased for the same energy budget as an eigenaxis maneuver. 2) By maneuvering off-eigenaxis, energy may be greatly decreased for the same slew time budget as a conventional eigenaxis maneuver.

The nonlinear relationship between slew time and energy, and the trade space between on- and off-eigenaxis maneuvering demonstrated in this paper, can be exploited for mission operations, planning, and design.

Appendix: Parameters for Example Spacecraft Used in This Paper

Table A1 Spacecraft parameters used in problem formulations defined in Sec. II

Parameter	Symbol	Value
Armature resistance	R	$1.8\,\Omega$
Motor torque constant	K_T	$0.0696\ \text{N}\cdot\text{m/A}$
Back EMF constant	K_V	$0.0696\ \text{V}(\text{rad/s})^{-1}$
Wheel viscous friction coefficient	β	$4.3\times10^{-5}\ \text{N}\cdot\text{m}(\text{rad/s})^{-1}$
Maximum reaction wheel speed	$\Omega_{\max}$	$450.0\ \text{rad/s}$
Maximum motor torque	$\tau_{\max}$	$0.14\ \text{N}\cdot\text{m/s}$
Wheel rotor inertia	J_{rw}	$0.012\ \text{kg}\cdot\text{m}^2$
Wheel speed bias	Ω_{bias}	$20.0\ \text{rad/s}$
Rate gyro limit	$\omega_{\max}$	$0.5\ \text{deg/s per axis}$
Wheel projection matrix	A	$\dfrac{1}{\sqrt{3}}\begin{bmatrix} 1 & -1 & -1 & 1 \\ 1 & -1 & 1 & -1 \\ 1 & 1 & -1 & -1 \end{bmatrix}$
Spacecraft inertia tensor	J_{sc}	$\begin{bmatrix} 59.22 & -1.14 & -0.80 \\ -1.14 & 40.56 & 0.10 \\ -0.80 & 0.10 & 57.60 \end{bmatrix}\ \text{kg}\cdot\text{m}^2$

References

[1] Scrivener, S. L., and Thompson, R. C., "Survey of Time-Optimal Attitude Maneuvers," *Journal of Guidance, Control, and Dynamics*, Vol. 17, No. 2, 1994, pp. 225–233.
doi:10.2514/3.21187

[2] Bilimoria, K. D., and Wie, B., "Time-Optimal Three-Axis Reorientation of a Rigid Spacecraft," *Journal of Guidance, Control, and Dynamics*, Vol. 16, No. 3, 1993, pp. 446–452.
doi:10.2514/3.21030

[3] Shen, H., and Tsiotras, P., "Time-Optimal Control of Axisymmetric Rigid Spacecraft Using Two Controls," *Journal of Guidance, Control, and Dynamics*, Vol. 22, No. 5, 1999, pp. 682–694.
doi:10.2514/2.4436

[4] Proulx, R., and Ross, I., "Time-Optimal Reorientation of Asymmetric Rigid Bodies," *Advances of the Astronautical Sciences*, Vol. 109, 2001, pp. 1207–1227.

[5] Fleming, A., "Real-Time Optimal Slew Maneuver Design and Control," M.S. Thesis, Naval Postgraduate School, Monterey, CA, 2004.

[6] Fleming, A., Sekhavat, P., and Ross, I. M., "Minimum-Time Reorientation of a Rigid Body," *Journal of Guidance, Control, and Dynamics*, Vol. 33, No. 1, 2010, pp. 160–170.
doi:10.2514/1.43549

[7] Fleming, A., and Ross, I. M., "Singularity-Free Optimal Steering of Control Moment Gyros," *Advances in the Astronautical Sciences*, Vol. 123, 2006, pp. 2681–2700.

[8] Fleming, A., and Ross, I. M., "Optimal Control of Spinning Axisymmetric Spacecraft: A Pseudospectral Approach," *AIAA Guidance, Navigation and Control Conference and Exhibit*, AIAA, Reston, VA, 2008, p. 7164.

[9] Fleming, A., Sekhavat, P., and Michael Ross, I., "Constrained, Minimum-Time Maneuvers for CMG Actuated Spacecraft," *Advances in the Astronautical Sciences*, Vol. 135, No. 2, 2009, pp. 1009–1027.

[10] Karpenko, M., Bhatt, S., Bedrossian, N., Fleming, A., and Ross, I. M., "First Flight Results on Time-Optimal Spacecraft Slews," *Journal of Guidance, Control, and Dynamics*, Vol. 35, No. 2, 2012, pp. 367–376.
doi:10.2514/1.54937

[11] Karpenko, M., Bhatt, S., Bedrossian, N., and Ross, I. M., "Flight Implementation of Shortest-Time Maneuvers for Imaging Satellites," *Journal of Guidance, Control, and Dynamics*, Vol. 37, No. 4, 2014, pp. 1069–1079.

[12] Schaub, H., and Lappas, V. J., "Redundant Reaction Wheel Torque Distribution Yielding Instantaneous L2 Power-Optimal Spacecraft

Attitude Control," *Journal of Guidance, Control, and Dynamics*, Vol. 32, No. 4, 2009, pp. 1269–1276.
doi:10.2514/1.41070

[13] Blenden, R., and Schaub, H., "Regenerative Power-Optimal Reaction Wheel Attitude Control," *Journal of Guidance, Control, and Dynamics*, Vol. 35, No. 4, 2012, pp. 1208–1217.
doi:10.2514/1.55493

[14] Dueri, D., Leve, F., and Açıkmeşe, B., "Minimum Error Dissipative Power Reduction Control Allocation via Lexicographic Convex Optimization for Momentum Control Systems," *IEEE Transactions on Control Systems Technology*, Vol. 24, No. 2, 2016, pp. 678–686.

[15] Wehrend, W. R., "Minimum Energy Reaction Wheel Control for a Satellite Scanning a Small Celestial Area," NASA TN D-392, 1967.

[16] Skaar, S., and Kraige, L., "Single-Axis Spacecraft Attitude Maneuvers Using an Optimal Reaction Wheel Power Criterion," *Journal of Guidance, Control, and Dynamics*, Vol. 5, No. 5, 1982, pp. 543–544.
doi:10.2514/3.56200

[17] Skaar, S., and Kraige, L., "Large-Angle Spacecraft Attitude Maneuvers Using an Optimal Reaction Wheel Power Criterion," *Journal of Astronautical Sciences*, Vol. 32, No. 1, 1984, pp. 47–61.

[18] Ross, I. M., and Karpenko, M., "A Review of Pseudospectral Optimal Control: From Theory to Flight," *Annual Reviews in Control*, Vol. 36, No. 2, 2012, pp. 182–197.
doi:10.1016/j.arcontrol.2012.09.002

[19] Schaub, H., *Analytical Mechanics of Space Systems*, AIAA Education Series, 3rd ed., AIAA, Reston, VA, 2003.

[20] Wie, B., *Space Vehicle Dynamics and Control*, AIAA Education Series, 2nd ed., AIAA, Reston, VA, 2008.

[21] Bialke, B., "High Fidelity Mathematical Modeling of Reaction Wheel Performance," *21st Annual American Astronautical Society Guidance and Control Conference*, American Astronautical Soc. Paper 98-063, 1998.

[22] Marsh, H., Karpenko, M., and Gong, Q., "Energy Constrained Shortest-Time Maneuvers for Reaction Wheel Satellites," *AIAA/AAS Astrodynamics Specialist Conference*, AIAA Paper 2016-5579, Sept. 2016.

[23] Wie, B., and Lu, J., "Feedback Control Logic for Spacecraft Eigenaxis Rotations Under Slew Rate and Control Constraints," *Journal of Guidance, Control, and Dynamics*, Vol. 18, No. 6, 1995, pp. 1372–1379.
doi:10.2514/3.21555

[24] Ross, I. M., and Fahroo, F., "Legendre Pseudospectral Approximations of Optimal Control Problems," *Lecture Notes in Control and Information Sciences*, Vol. 295, Springer–Verlag, New York, 2003, pp. 327–342.

[25] Gong, Q., Kang, W., and Ross, I. M., "A Pseudospectral Method for the Optimal Control of Constrained Feedback Linearizable Systems," *IEEE Transactions on Automatic Control*, Vol. 51, No. 7, 2006, pp. 1115–1129.
doi:10.1109/TAC.2006.878570

[26] Kang, W., Gong, Q., and Ross, I. M., "Convergence of Pseudospectral Methods for a Class of Discontinuous Optimal Control," *Proceedings of the 44th IEEE Conference on Decision and Control*, IEEE Publ., Piscataway, NJ, 2005, pp. 2799–2804.

[27] Ross, I. M., *A Primer on Pontryagin's Principle in Optimal Control*, 2nd ed., Collegiate Publ., San Francisco, 2015.

[28] Ross, I. M., "A Historical Introduction to the Covector Mapping Principle," *AAS/AIAA Astrodynamics Specialist Conference*, AAS Paper 05-332, Lake Tahoe, CA, Aug. 2005.

[29] Gong, Q., Ross, I. M., Kang, W., and Fahroo, F., "Connections Between the Covector Mapping Theorem and Convergence of Pseudospectral Methods for Optimal Control," *Computational Optimization and Applications*, Vol. 41, No. 3, 2008, pp. 307–335.
doi:10.1007/s10589-007-9102-4

[30] Gong, Q., Ross, I. M., and Fahroo, F., "Costate Computation by a Chebyshev Pseudospectral Method," *Journal of Guidance, Control, and Dynamics*, Vol. 33, No. 2, 2010, pp. 623–628.
doi:10.2514/1.45154

[31] Bedrossian, N., Karpenko, M., and Bhatt, S., "Overclock My Satellite," *IEEE Spectrum*, Vol. 49, No. 11, 2012, pp. 54–62.
doi:10.1109/MSPEC.2012.6341207